BİNGÖL UNIVERSITY

Turkish Journal of Nature and Science

e-ISSN: 2149-6366
www.dergipark.gov.tr/tdfd

Research Article

Volume 15, Issue 2, Page 154-163, 2026

Received: 17.02.2026
Accepted: 29.04.2026
Published: 30.06.2026

DOI: https://doi.org/10.46810/tdfd.1891540

Structural and Mechanical Characterization of Natural Fluoroapatite/3Y-TZP Composites Consolidated by Spark Plasma Sintering

Burak DEMİR[1*]

[1]Bingol University, Faculty of Engineering and Architecture, Mechanical Engineering Department, Bingöl, Türkiye

Corresponding author: bdemir@bingol.edu.tr

Abstract

This study investigates the structural and mechanical properties of natural fluoroapatite (FAP)/3 mol% yttria-stabilized zirconia (3YSZ) composites consolidated by spark plasma sintering (SPS). Powder mixtures containing 0–100 vol.% 3YSZ were prepared and sintered at optimized temperatures between 800 and 1300 °C under 50 MPa for 10 min. Phase composition, microstructure, density, hardness, and fracture toughness were systematically characterized using XRD, SEM-EDS, Archimedes' method, and Vickers indentation. High relative densities (96–99%) were achieved within short sintering times. XRD results confirmed the coexistence of tetragonal YSZ and hexagonal FAP phases without detectable secondary phases. Microstructural analysis revealed a homogeneous distribution of YSZ within the FAP matrix. Mechanical properties increased with YSZ content. Pure YSZ exhibited the highest hardness (13.66 GPa) and fracture toughness (5.52 MPa.m$^{0.5}$), while the 95YSZ–5FAP composite retained relatively high mechanical performance (13.46 GPa, 4.42 MPa.m$^{0.5}$). Higher FAP contents led to significant reductions in toughness. The results demonstrate that SPS enables dense bioactive composites while preserving the mechanical integrity of zirconia-rich compositions.

Keywords

Fluorapatite,
ZrO2,
YSZ,
SPS,
composite

BİNGÖL ÜNİVERSİTESİ

Türk Doğa ve Fen Dergisi

e-ISSN: 2149-6366
www.dergipark.gov.tr/tdfd

Araştırma Makalesi

Cilt 15, Sayı 2, Sayfa 154-163, 2026

Alınış: 17.02.2026
Kabul: 29.04.2026
Basım: 30.06.2026

DOI: https://doi.org/10.46810/tdfd.1891540

Spark Plazma Sinterleme Yöntemiyle Yoğunlaştırılan Doğal Florapatit / 3Y-TZP Kompozitlerinin Yapısal ve Mekanik Özelliklerinin İncelenmesi

Burak DEMİR[1*]

[1]Bingöl Üniversitesi, Mühendislik ve Mimarlık Fakültesi, Makine Mühendisliği Bölümü, Bingöl, Türkiye

**Sorumlu yazar: bdemir@bingol.edu.tr*

Özet

Bu çalışmada, spark plazma sinterleme (SPS) yöntemi ile sinterlenen doğal fluoroapatit (FAP) ve %3 mol itriya ile stabilize edilmiş zirkonya (3YSZ) kompozitlerinin yapısal ve mekanik özellikleri incelenmiştir. Hacimce %0–100 oranlarında 3YSZ içeren toz karışımları hazırlanmış ve 50 MPa basınç altında 10 dakika süreyle 800–1300 °C arasındaki optimize edilmiş sinterleme sıcaklıklarında sinterlenmiştir. Faz bileşimi, mikroyapı, yoğunluk, sertlik ve kırılma tokluğu; XRD, SEM-EDS, Arşimet yöntemi ve Vickers indentasyon analizleri kullanılarak sistematik olarak karakterize edilmiştir. Kısa sinterleme sürelerinde görece yüksek yoğunluk değerleri (%96–99) elde edilmiştir. XRD sonuçları, herhangi bir ikincil faz oluşumu tespit edilmeden tetragonal YSZ ve hekzagonal FAP fazlarının birlikte bulunduğunu doğrulamıştır. Mikroyapısal analizler, YSZ fazının FAP matrisi içinde homojen bir şekilde dağıldığını göstermiştir. Mekanik özellikler, YSZ içeriğinin artmasıyla birlikte iyileşmiştir. Saf YSZ en yüksek sertlik (13,66 GPa) ve kırılma tokluğu (5,52 MPa.m^{0,5}) değerlerini sergilerken, %95 YSZ–%5 FAP kompoziti nispeten yüksek mekanik performansını korumuştur (13,46 GPa, 4,42 MPa.m^{0,5}). Daha yüksek FAP içerikleri ise kırılma tokluğunda belirgin azalmalara yol açmıştır. Sonuçlar, SPS yönteminin zirkonya açısından zengin bileşimlerin mekanik bütünlüğünü korurken yoğun ve biyouyumlu kompozitlerin üretimine olanak sağladığını göstermektedir.

Anahtar kelimeler

Florapatit,
ZrO2,
YSZ,
SPS,
kompozit

1. INTRODUCTION

Due to contemporary changes in dietary habits, maintaining long-term dental health has become increasingly challenging, leading to a steady rise in the demand for dental implants. Consequently, extensive research efforts have been directed in recent years toward the development of biocompatible and mechanically durable implant materials [1]. The clinical success of dental materials used in oral rehabilitation is governed by the synergistic interplay of high mechanical strength under masticatory loads, chemical stability in the oral environment, and advanced biocompatibility with surrounding tissues [2]. Although metals, polymers, and ceramics are widely employed in current dental applications, an ideal restorative material is expected to simultaneously exhibit an elastic modulus close to that of natural tooth tissue, high fracture toughness, and low density [3]. However, the inherent brittleness of conventional monolithic ceramics and the insufficient tissue integration of bioinert materials remain among the primary causes of clinical failure. To overcome these limitations, ceramic–ceramic composite structures have been developed to integrate the complementary advantages of different phases, enabling the concurrent optimization of mechanical and biological performance [4]. In particular, the application of advanced powder metallurgy techniques such as Spark Plasma Sintering (SPS) enables full densification at significantly lower temperatures and shorter processing times compared to conventional methods, thereby suppressing grain growth and maximizing the microstructural stability of dental composites [5].

Modern dental restorations rely heavily on zirconia (ZrO_2) as a core structural material, which is often referred to as “ceramic steel” due to its polymorphic crystal structure and the resulting mechanical advantages [6]. Pure zirconia undergoes temperature-dependent phase transformations among monoclinic, tetragonal, and cubic structures; however, in dental applications, the tetragonal phase zirconia (t-ZrO_2) stabilized with oxides, such as yttria (Y_2O_3) is of critical importance [7]. The most prominent advantage of this material lies in the transformation toughening mechanism, in which the tetragonal phase transforms into the monoclinic phase with an associated volumetric expansion during crack propagation, thereby inducing compressive stresses at the crack tip and effectively hindering further crack growth [8]. With a high flexural strength in the range of approximately 900–1200 MPa and a theoretical density of about 6.08 $g.cm^{-3}$, zirconia has become an indispensable framework material, particularly for posterior regions subjected to high masticatory loads [9].

Despite the outstanding mechanical performance of zirconia, its biologically inert character prevents the formation of a chemical bond with surrounding tissues, thereby restricting its clinical functionality primarily to morphological retention [10]. To overcome this limitation, zirconia–fluorapatite [$Ca_{10}(PO_4)_6F_2$] composite systems have been developed with the aim of integrating the mechanical strength of zirconia with bioactive functionality [11]. Fluorapatite offers excellent biocompatibility owing to its structural similarity to the primary mineral components of natural tooth enamel and bone, while exhibiting lower solubility and higher chemical stability in acidic oral environments compared to hydroxyapatite [12].

Despite the biological advantages provided by fluorapatite, its inherent mechanical limitations, such as low fracture toughness and poor tensile strength, render it unsuitable for use as a standalone load-bearing material in dental restorations [13]. Preserving the mechanical integrity of the fluorapatite phase within a zirconia matrix while achieving full densification is particularly challenging using conventional sintering methods, as prolonged exposure to high temperatures may lead to chemical degradation of fluorapatite or excessive grain growth in zirconia, ultimately resulting in a loss of toughness [14].

In this context, Spark Plasma Sintering (SPS) offers a transformative solution by drastically reducing sintering times to the order of minutes through the application of very high heating rates and external pressure. The SPS technique enables high densification even at relatively low temperatures, thereby preventing the thermal degradation of fluorapatite, limiting grain growth, preserving microstructural homogeneity, and ultimately facilitating the fabrication of dental composites that are both bioactive and mechanically robust [15]. In this context, the present study aims to fabricate zirconia–fluorapatite ceramic composites via Spark Plasma Sintering and to systematically evaluate the influence of SPS processing on densification behavior, phase formation, microstructural characteristics, and the resulting mechanical performance.

2. MATERIAL AND METHOD

2.1. Material

In this study, natural fluorapatite (FAP) powder (natural source from Mazıdagi/Mardin, Turkiye) and commercially available 3 mol% yttria-stabilized tetragonal zirconia (3YSZ, TOSOH, Japan) were used as starting materials. Prior to powder mixing, the natural fluorapatite was calcined at 850 °C for 3 h in atmospheric conditions to remove volatile species and improve phase stability [16].

2.2. Preperation of Powders

Natural fluorapatite and 3 mol% yttria-stabilized tetragonal zirconia powders were mixed in a roll mill for 24 h at a rotational speed of 60 rpm. Powder compositions were prepared with volumetric ratios of 0, 5, 25, 50, 75, 95, and 100 vol.% 3YSZ. The corresponding mixture ratios and sample codes are presented in Table 1.

2.3. Sintering of Composites

The sintering temperatures of fluorapatite and yttria-stabilized zirconia differ significantly; while fluorapatite

tends to decompose at excessively high temperatures, zirconia does not achieve sufficient densification at low temperatures. Therefore, all compositions were sintered at optimized temperatures suitable for both phases. Spark Plasma Sintering (SPS) was employed for the consolidation of 3YSZ–FAP composites using an SPS furnace (HPD 25, FCT System, Germany). Homogeneously mixed powders were loaded into graphite dies with a diameter of 20 mm. To minimize interactions between the powders and the graphite die, graphite foil was placed between the powder and the die walls. After uniaxial pre-pressing using a manual press, the graphite die was wrapped with a graphite blanket and placed inside the SPS chamber. SPS processing was carried out at temperatures ranging from 800 to 1300 °C under an applied pressure of 50 MPa, with heating and cooling rates of 100 °C min^{-1} and a dwell time of 10 min. Following SPS sintering, residual carbon layers on the pellet surfaces were removed using a diamond cutting disc. The detailed SPS parameters for all samples are summarized in Table 2.

2.4. Characterization

The densities of the SPS-sintered composites were determined using the Archimedes principle. The presence of SiO2 and larnite phases in the natural fluorapatite was neglected, as their contents were sufficiently low to have a negligible effect on the overall density. The measured densities of all samples are listed in Table 1.

Semi-quantitative phase analyses of the samples were conducted by X-ray diffraction (XRD) over a 2θ range of 10–65° using an X-ray diffractometer (Ultima IV, Rigaku) operated at 40 kV and 30 mA, with a step size of 0.02° and a scanning rate of 4° min^{-1}. Peak identification was performed using the integrated PDXL X-ray powder diffraction software.

Microstructural observations were carried out on polished cross-sections using a scanning electron microscope (SEM, Supra 50VP, Zeiss) operated in backscattered electron (BSE) mode. Elemental compositions were analyzed at selected points, lines, and areas using an energy-dispersive X-ray spectroscopy (EDS) detector integrated into the SEM (Oxford Instruments).

Vickers indentation hardness measurements were performed on polished cross-sections using an Emcotest M1C hardness tester (Emcotest, Germany) under an applied load of 5 kg (HV5). At least five indentations were made at different locations on each sample, and the hardness values were calculated using the following equation (Equation 1):

$$HV = 1.8544.F.d^{-2} \quad (1)$$

where F is the applied load (N) and d is the average length of the two indentation diagonals (mm).

The fracture toughness (K_{IC}) was calculated from the radial cracks generated around the Vickers indentations using the Evans and Charles model (Equation 2) [17, 18]:

$$K_{IC} = 0.16\ (c.a^{-1})\ (-1.5)\ (H.a^{0.5}) \quad (2)$$

where K_{IC} is the fracture toughness (MPa $m^{0.5}$), H is the Vickers hardness (MPa), c is the average crack length (μm), and a is the average half-diagonal length of the indentation (μm).

3. RESULTS AND DISCUSSION

3.1. Phase and Microstructural Analysis

The natural fluorapatite primarily consists of fluorapatite as the main phase, accompanied by minor phases such as SiO_2 and $CaCO_3$ [19]. Prior to powder mixing, the natural fluorapatite was calcined at 850 °C for 3 h. During calcination, $CaCO_3$ decomposed into CaO and CO2 (g), after which SiO_2 reacted with CaO to form the larnite phase [20]. Following calcination, trace amounts of SiO_2 and larnite phases remained within the fluorapatite structure. However, due to their very low concentrations, these phases are not expected to adversely affect either the potential biocompatibility or the structural integrity of the material.

After powder mixing, the powders were loaded into graphite dies and sintered at various temperatures using SPS. The SPS parameters for all samples are summarized in Table 1. It is noted that some compositions were sintered at multiple temperatures, with the aim of achieving the highest possible relative density for each powder mixture. The sintering temperatures and dwell times were optimized by monitoring the displacement rate of the SPS piston to identify the onset and completion of densification. For the 95YSZ-5FAP composition, iterative trials were conducted at three different temperatures to determine the parameters that yielded the highest relative density. This systematic approach ensured that each composite was fabricated under its optimal processing window.

Figure 1 presents the SPS graphs, illustrating temperature-piston displacement curves as a function of time. As representative examples, Figures 1e and 1f show two different SPS curves for the 75YSZ–25FAP composition. At a sintering temperature of 1130 °C, incomplete neck formation and insufficient densification are observed, whereas at 1190 °C, the completion of neck formation and the attainment of a high densification level are evident from the sintering curve. The relative densities of the samples sintered at 1130 °C and 1190 °C were calculated as 93.7% and 95.7%, respectively. Examination of the remaining samples reveals that densification initiates at specific temperatures, followed by the formation of a plateau region during the dwell stage, indicating the completion of densification. Pure fluorapatite begins to densify at approximately 700 °C, while pure YSZ starts to densify at around 1150 °C. Compared to conventional sintering methods, SPS enables the achievement of higher densities at lower temperatures and significantly shorter processing times. Accordingly, relative densities in the range of 96–99% were obtained for all samples within a dwell time of only 10 min (Table 2). It should be noted that the high relative density values obtained (96-99%)

may contain a minor margin of error, as the theoretical density calculations primarily focused on the main phases and did not account for the trace amounts of impurities such as SiO_2 and larnite present in the fluorapatite content. However, given the minimal volume fraction of these secondary phases, this exclusion is not expected to significantly alter the overall densification trends observed.

The XRD patterns of the SPS-sintered composites are shown in Figure 2. For the pure fluorapatite sample, only diffraction peaks corresponding to hexagonal fluorapatite are observed (PDF card no. 71-0880) [21]. Diffraction peaks associated with SiO_2 and larnite phases could not be detected due to their very low concentrations. In the 3YSZ sample, only diffraction peaks corresponding to the tetragonal YSZ phase are present (PDF card no. 01-083-0113) [22], confirming that zirconia is fully stabilized in the tetragonal form without the presence of secondary phases. In the YSZ–FAP composites, diffraction peaks corresponding to both constituent phases are clearly identified, indicating the coexistence of fluorapatite and tetragonal zirconia.

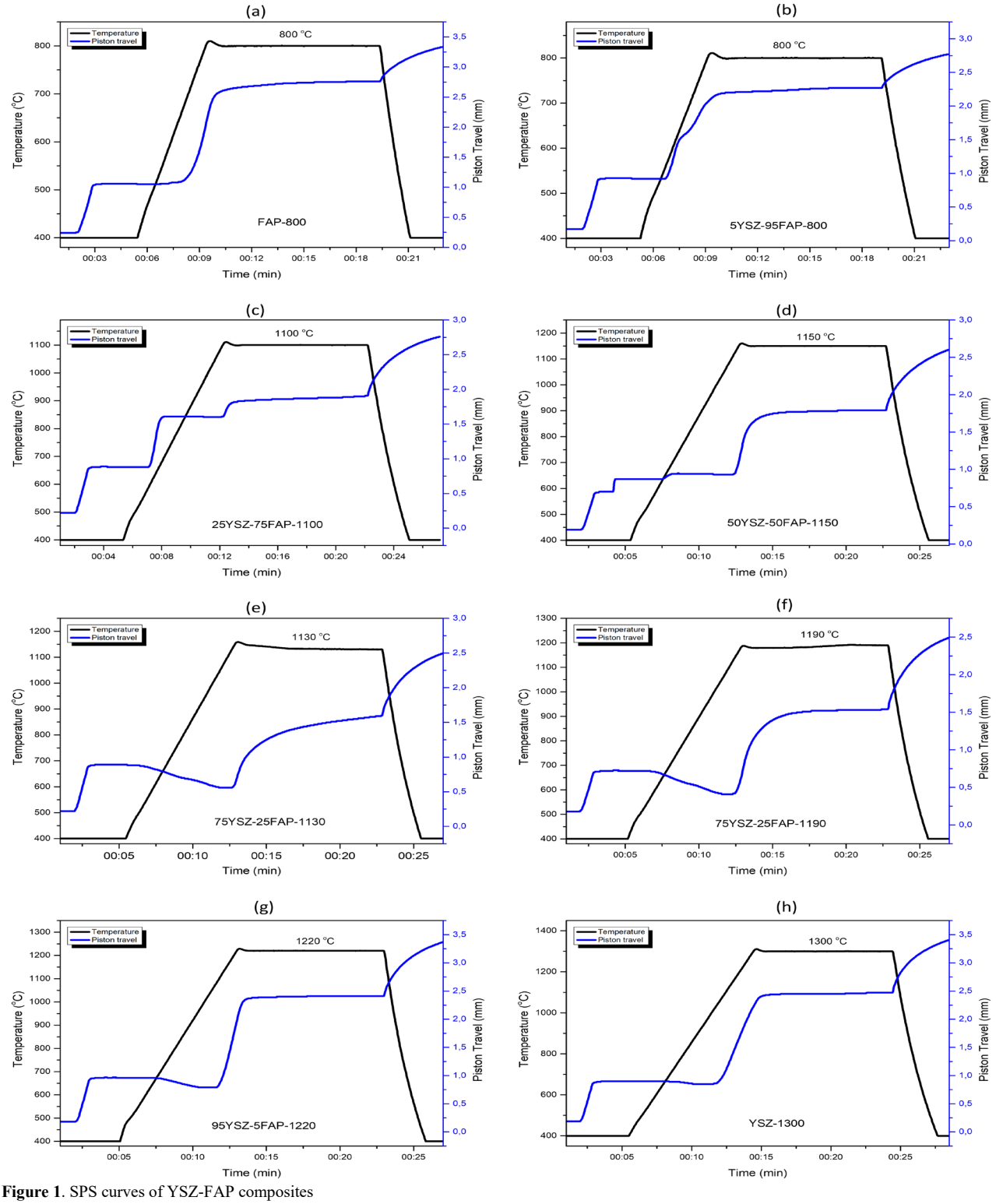

Figure 1. SPS curves of YSZ-FAP composites

Table 1. SPS parameters of homogenously mixed FAP-YSZ composites.

Sample	Temperature (°C)	Pressure (MPa)	Dwell time (min)	Heating/Cooling rate (°C/min)
FAP-800	800	50	10	100/100
5YSZ-95FAP-800	800	50	10	100/100
25YSZ-75FAP-1000	1000	50	10	100/100
25YSZ-75FAP -1100	1100	50	10	100/100
50YSZ-50FAP-1050	1050	50	10	100/100
50YSZ-50FAP-1150	1150	50	10	100/100
75YSZ-25FAP-1130	1130	50	10	100/100
75YSZ-25FAP -1180	1190	50	10	100/100
95YSZ-5FAP -1200	1200	50	10	100/100
95YSZ-5FAP -1210	1210	50	10	100/100
95YSZ-5FAP -1220	1220	50	10	100/100
YSZ-1300	1300	50	10	100/100

Table 2. Comparison of density and mechanical properties of FAP, YSZ, and YSZ-FAP composites

Samples	Density (g/cm^3)	Relative Density (%)	Hardness (GPa)	Fracture Toughness (MPa.m$^{1/2}$)
FAP-800	3.152	99.2	5.50	1.12
5YSZ-95FAP-800	3.267	98.1	5.52	1.11
25YSZ-75FAP-1000	3.701	94.1		
25YSZ-75FAP -1100	3.813	96.9	5.67	1.23
50YSZ-50FAP-1050	4.393	93.7		
50YSZ-50FAP-1150	4.509	96.1	9.12	1.56
75YSZ-25FAP-1130	5.102	93.7		
75YSZ-25FAP -1190	5.210	95.7	12.15	2.24
95YSZ-5FAP -1200	5.597	92.5		
95YSZ-5FAP -1210	5.819	96.2	12.91	4.22
95YSZ-5FAP -1220	5.910	97.7	13.46	4.42
YSZ-1300	6.092	98.3	13.66	5.52

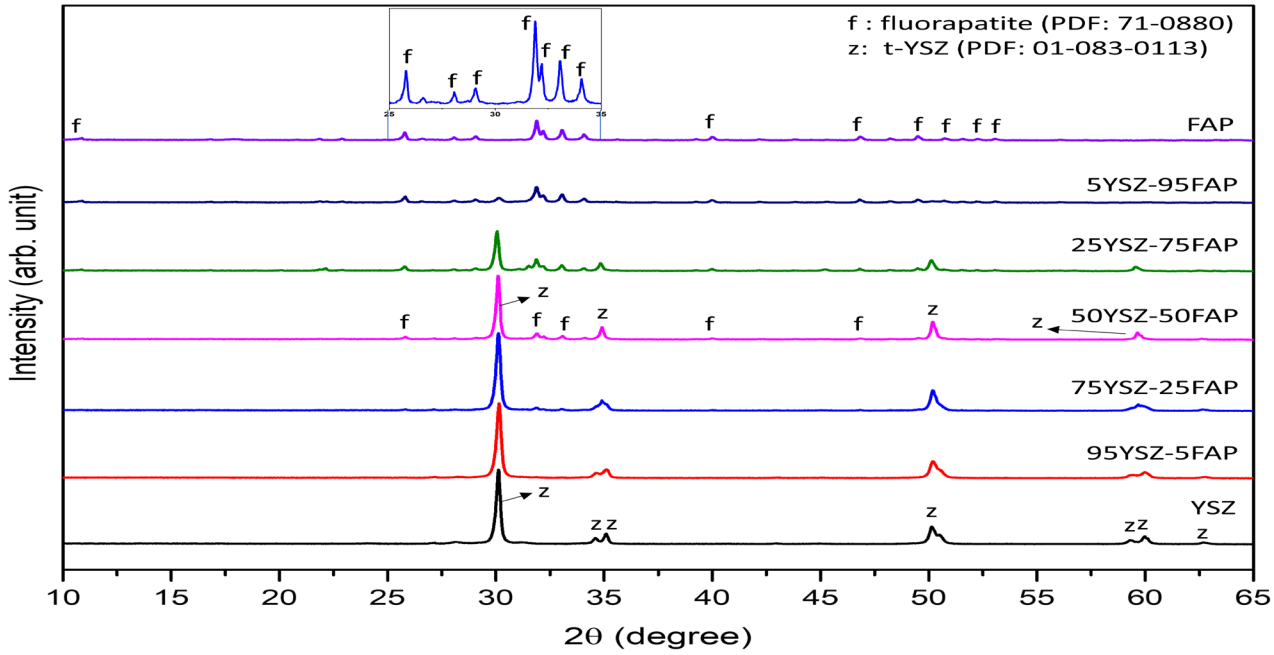

Figure 2. XRD patterns of YSZ-FAP composites after sintering

Figure 3 presents low- and high-magnification microstructural images of the YSZ-1300 and 95YSZ–5FAP-1300 samples. As observed, both samples exhibit nearly pore-free microstructures after sintering, with only a small number of isolated micropores distributed throughout the structure. The relative density of the YSZ sample sintered at 1300 °C was calculated as 98.3%. The EDS analysis of the YSZ-1300 sample, shown in Figure 3(a3), reveals Zr, Y, and O contents of 32.54%, 0.95%, and 66.5%, respectively, confirming that the material corresponds to 3 mol% yttria-stabilized zirconia. The relative density of the 95YSZ–5FAP sample sintered at 1220 °C was calculated as 97.7%. The absolute and relative densities of all samples are listed in Table 1. During the calculation of relative density, trace impurities present in fluorapatite were neglected, and zirconia was considered as 3 mol% yttria-stabilized. Microstructural examination of the 95YSZ–5FAP composite reveals dark particles with sizes ranging from approximately 0.5 to 3 μm dispersed within the matrix.

These particles exhibit irregular morphologies, with some elongated grains showing aspect ratios of approximately 3–5, while smaller particles appear more equiaxed.

Figure 4 presents the EDS analysis results of the 95YSZ–5FAP-1220 sample. As shown by the elemental mapping in Figure 4a, Ca-rich regions (green) are localized within the dark contrast areas, whereas Zr (red) is predominantly distributed throughout the matrix phase, indicating that the matrix corresponds to YSZ and the dark regions correspond to fluorapatite. A line-scan EDS analysis across both the matrix and dark particles, shown in Figure 4b, reveals an increase in Ca intensity accompanied by a decrease in Zr intensity within the dark regions. Furthermore, point EDS analysis shown in Figure 4c confirms the presence of Ca, P, F, and O in the dark regions, while a high Zr concentration is detected in the matrix. These results collectively demonstrate that fluorapatite particles are uniformly dispersed within a 3YSZ matrix.

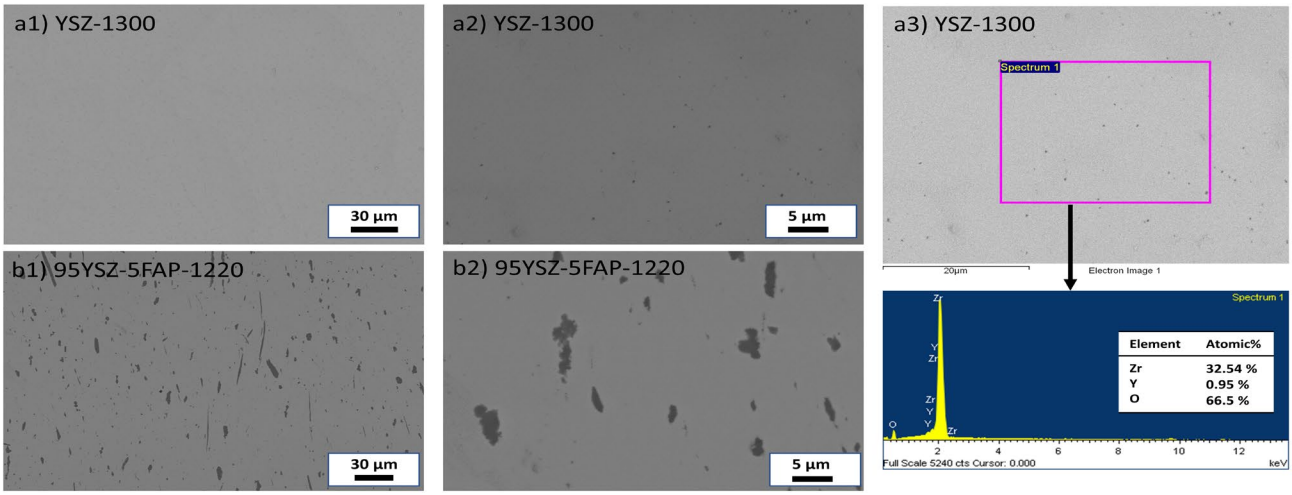

Figure 3. SEM micrographs of YSZ and 95YSZ-5FAP samples and EDS analysis of selected area of YSZ

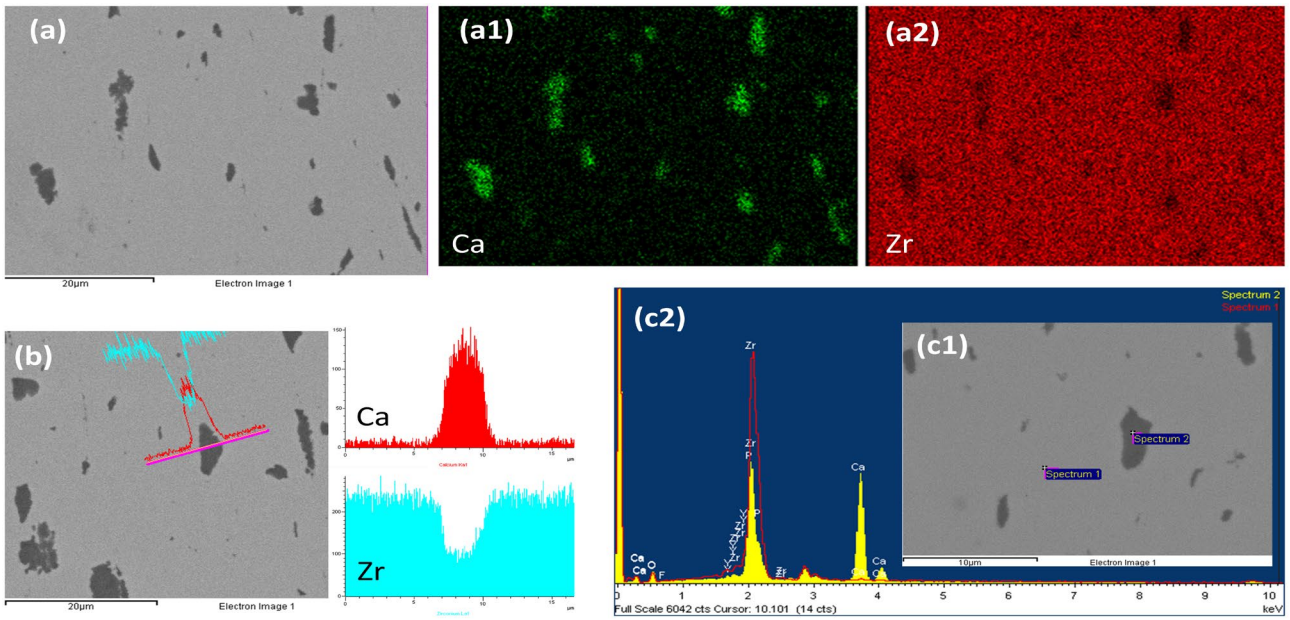

Figure 4. a) EDS mapping analysis of 95YSZ-5FAP sample b) EDS line analysis and c) EDS spot analysis from selected points

3.2. Mechanical Behaviour

The Vickers hardness (microhardness) and fracture toughness values of the fabricated samples are presented in Figure 5. The hardness and fracture toughness of undoped fluorapatite were measured as 5.5 GPa and 1.12 MPa.m$^{0.5}$, respectively, which are far below the values required for load-bearing implant applications [23]. The primary objective of this study was to combine the mechanical strength of YSZ with the biocompatibility of fluorapatite in order to produce an optimized composite material. As the YSZ content increases, both the hardness and fracture toughness of the composites show a corresponding increase. As expected [24], the highest hardness (13.66 GPa) and fracture toughness (5.52 MPa.m$^{0.5}$) were obtained for the monolithic YSZ-1300 sample. Although the incorporation of YSZ leads to improvements in both hardness and fracture toughness, only two samples are considered to meet the minimum mechanical requirements for implant applications [25], namely the YSZ and 95YSZ–5FAP samples, which exhibit

hardness values above 13 GPa and fracture toughness values exceeding 4 MPa.m$^{0.5}$. A pronounced decrease in fracture toughness is observed for samples containing 25 vol.% or more fluorapatite.

Overall, the mechanical behavior of the YSZ–FAP composites follows a rule-of-mixtures trend, indicating that a high YSZ content is required to preserve the superior mechanical properties of zirconia. The Vickers indentation imprints of the YSZ-1300 and 95YSZ–5FAP-1220 samples are shown in Figures 6(a1) and 6(b1), respectively. In both samples, well-defined diamond-shaped Vickers imprints are observed, accompanied by radial cracks emanating from the indentation corners. Crack propagation images of the YSZ-1300 sample and the 95YSZ–5FAP-1220 composite are shown in Figures 6(a2) and 6(b2–4), respectively. In the YSZ-1300 sample, no secondary toughening mechanisms capable of arresting crack propagation beyond the intrinsic mechanisms of YSZ are observed. In contrast, the composite contains fluorapatite particles dispersed within the YSZ matrix; however, when the propagating crack encounters a fluorapatite particle, neither crack deflection nor crack bridging mechanisms are activated. Contrary to expectations [26], the presence of fluorapatite locally weakens the intrinsic toughening mechanisms of YSZ, resulting in reduced crack energy dissipation and accelerated crack propagation. The reduction in fracture toughness is primarily linked to the coefficient of thermal expansion (CTE) mismatch between the matrix and reinforcement. This discrepancy generates residual stresses during cooling, facilitating microcrack initiation. Furthermore, insufficient interfacial bonding between YSZ and FAp limits toughening mechanisms like crack bridging, leading to preferential crack growth along the interfaces [27]. Consequently, the addition of fluorapatite leads to a reduction in both hardness and fracture toughness relative to monolithic YSZ. Nevertheless, due to the rapid densification achieved by SPS without excessive grain growth, the mechanical performance of the produced composites is superior to that of comparable materials fabricated using conventional sintering methods.

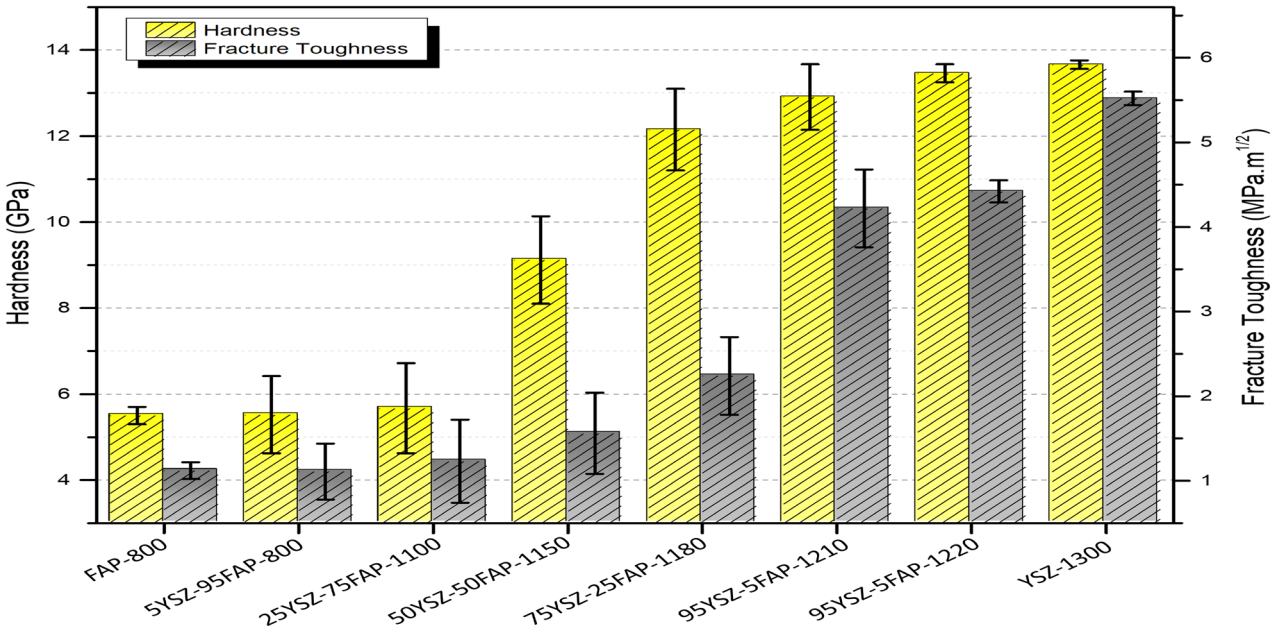

Figure 5. Hardness and fracture toughness graphs of YSZ-FAP composites

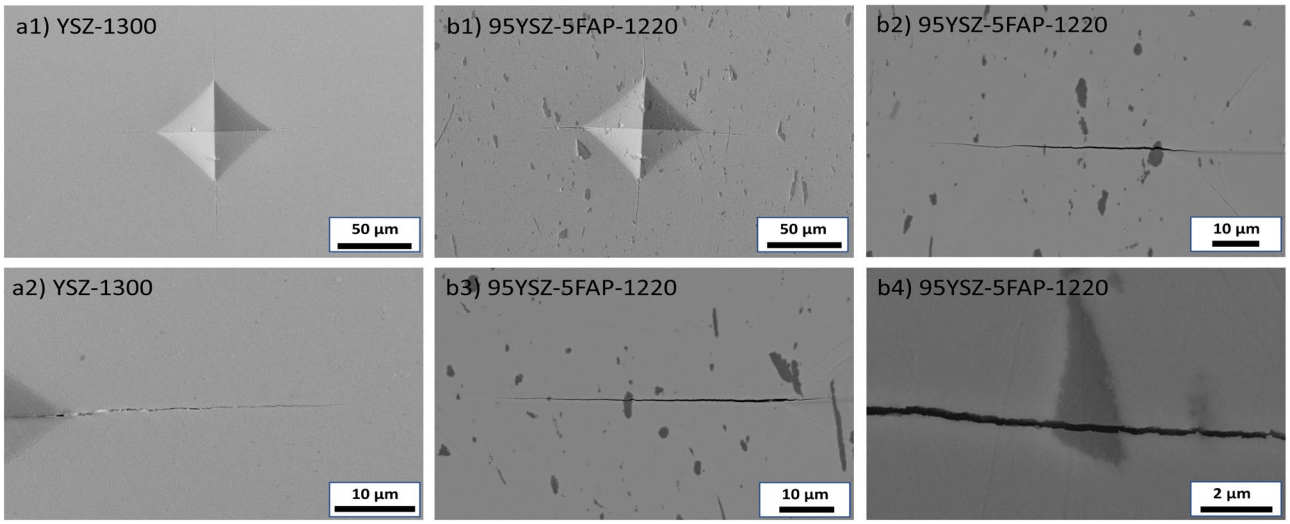

Figure 6. Micrographs of indents and crack propagation of a) YSZ and b) 95YSZ-5FAP samples

4. CONCLUSION

In this study, dense FAP/3YSZ composites were successfully fabricated using spark plasma sintering and systematically evaluated their phase stability, densification behavior, microstructural evolution, and mechanical performance. The results showed that SPS enabled rapid densification (96–99% relative density) while maintaining distinct tetragonal YSZ and hexagonal FAP phases without detrimental secondary reactions. Mechanical properties were strongly dependent on composition, following a rule-of-mixtures trend. Increasing FAP content reduced hardness and fracture toughness, whereas zirconia-rich compositions preserved superior mechanical behavior. Among the composites, the 95YSZ–5FAP sample provided a balance between mechanical strength (hardness and fracture toughness are 13 GPa and 4 $MPa.m^{0.5}$) and potential bioactivity, while pure YSZ exhibited the highest mechanical performance.

These findings contribute to the development of bioactive zirconia-based dental composites consolidated via rapid sintering routes. For load-bearing dental applications, zirconia-rich compositions are recommended. Future studies should focus on in vitro bioactivity, long-term degradation behavior, and optimization of FAP particle size and distribution to enhance toughening efficiency while maintaining biological functionality.

REFERENCES

[1] Aktas B, Das R, Acıkgoz A, Ulas EO, Demircan G, Uyar E, et al. Fabrication of $CaSiO_3$-doped 3Y-ZrO_2 ceramics via DLP 3D printing: Structural, mechanical, and biological evaluation. Journal of Alloys and Compounds. 2025;1036:181895.

[2] Gu Q, Yuan R, Sun D, Wallace G. Future Frontiers in Bioinspired Implanted Biomaterials. Advanced Materials. 2025;37(36):e06323.

[3] Ahmed MMS, Rabbi SF, Hossen MZ, Islam S, Sarker MAH, Hossain N, et al. Recent Advances in Biocompatible Dental Materials. Biomedical Materials & Devices. 2026:1–36.

[4] Ferreira C, Santiago A, Vasconcelos R, Paiva D, Pirih F, Araújo A, et al. Study of microstructural, mechanical, and biomedical properties of zirconia/hydroxyapatite ceramic composites. Ceramics International. 2022;48(9):12376–86.

[5] Demir B, Duden EI, Ayas E. Characterization of MoAlB ceramics synthesized via spark plasma sintering with Si addition and SiC reinforcement. Journal of Alloys and Compounds. 2023;953:170115.

[6] Alqutaibi AY, Ghulam O, Krsoum M, Binmahmoud S, Taher H, Elmalky W, et al. Revolution of current dental zirconia: A comprehensive review. Molecules. 2022;27(5):1699.

[7] Cesar PF, de Paula Miranda RB, Santos KF, Scherrer SS, Zhang Y. Recent advances in dental zirconia: 15 years of material and processing evolution. Dental Materials. 2024;40(5):824–36.

[8] Mamivand, M., M.A. Zaeem, and H. El Kadiri, Phase field modeling of stress-induced tetragonal-to-monoclinic transformation in zirconia and its effect on transformation toughening. Acta materialia, 2014. 64: p. 208-219.

[9] Huang B, Chen M, Wang J, Zhang X. Advances in zirconia-based dental materials: Properties, classification, applications, and future prospects. Journal of Dentistry. 2024;147:105111.

[10] Osman RB, Swain MV, Atieh M, Ma S, Duncan W. Ceramic implants (Y-TZP): are they a viable alternative to titanium implants for the support of overdentures? A randomized clinical trial. Clinical Oral Implants Research. 2014;25(12):1366–77.

[11] Nasiri-Tabrizi B, Fahami A. Synthesis and characterization of fluorapatite–zirconia composite nanopowders. Ceramics International. 2013;39(4):4329–37.

[12] Pajor K, Pajchel L, Kolmas J. Hydroxyapatite and fluorapatite in conservative dentistry and oral implantology—A review. Materials. 2019;12(17):2683.

[13] Bouslama N, Ayed FB, Bouaziz J. Sintering and mechanical properties of tricalcium phosphate–fluorapatite composites. Ceramics International. 2009;35(5):1909–17.

[14] Cao Y, Li C, Xia Y, Ren K, Zhu S. Study on the fabrication and mechanical properties of HAp-3YSZ composites by flash sintering. Ceramics International. 2022;48(11):16300–5.

[15] Tokita M. Progress of spark plasma sintering (SPS) method, systems, ceramics applications and industrialization. Ceramics. 2021;4(2):160–98.

[16] Demir B, Ayas E. Effects of sintering temperature and doping content on luminescence properties of rare earth (Sm^{3+}, Eu^{3+}, and Dy^{3+}) doped natural fluorapatite. Journal of Solid State Chemistry. 2022;306:122783.

[17] Demir B. Novel $MoSi_2$–MoB_2 composites: Single-step in-situ synthesis from elemental powders via spark plasma sintering. Journal of Alloys and Compounds. 2025:185651.

[18] Evans AG, Charles EA. Fracture toughness determinations by indentation. Journal of the American Ceramic Society. 1976;59(7–8):371–2.

[19] Demir B, Derince D, Dayioglu T, Koroglu L, Karacaoglu E, Uz V, et al. Effects of doping content and crystallite size on luminescence properties of Eu^{3+} doped fluorapatites obtained from natural waste. Ceramics International. 2021;47(24):34657–66.

[20] Demir B, Karacaoglu E, Agil AA, Koroglu L, Ayas E. Effect of Gd-codoping on photoluminescence properties of Eu-doped natural fluorapatite. Optik. 2023;287:171123.

[21] Demir B, İmak A, Karacaoğlu E. Enhancing the photoluminescence performance of Sm-doped

fluorapatite with Dy co-doping. Ceramics International. 2025.

[22] Bartolomé JF, Smirnov A, Kurland H-D, Grabow J, Müller FA. New ZrO_2/Al_2O_3 nanocomposite fabricated from hybrid nanoparticles prepared by CO_2 laser co-vaporization. Scientific Reports. 2016;6(1):20589.

[23] Flanagan D. Bite force and dental implant treatment: A short review. Medical Devices: Evidence and Research. 2017:141–8.

[24] Kim DS, Lee JK. Sintered characteristics of 3 mole% yttria-stabilized zirconia polycrystals (3Y-TZP) implants manufactured by slip-casting and computer aided design/computer aided manufacturing (CAD/CAM). Journal of Nanoscience and Nanotechnology. 2021;21(7):3877–81.

[25] Abraham AM, Venkatesan S. A review on application of biomaterials for medical and dental implants. Proceedings of the Institution of Mechanical Engineers, Part L: Journal of Materials: Design and Applications. 2023;237(2):249–73.

[26] Adolfsson E, Hermansson L. Zirconia–fluorapatite materials produced by HIP. Biomaterials. 1999;20(14):1263–7.

[27] Durmuşoğlu Ş, Altuner EE. Synthesis and Characterization of Erbia - Doped Yttria - Stabilized Ceria - Zirconia Based Nanoceramics. Turkish Journal of Nature and Science, 2025; 14(4), 158-164